energies

MDPI

Article

An Experimental and Kinetic Modelling Study on Laminar Premixed Flame Characteristics of Ethanol/Acetone Mixtures

Yangxun Liu [1], Weinan Liu [2], Huihong Liao [3], Wenhua Zhou [2] and Cangsu Xu [2,*]

[1] Zhejiang Technical Institute of Economics, Hangzhou 310018, China; 240064@zjtie.edu.cn
[2] College of Energy Engineering, Zhejiang University, Hangzhou 310027, China; 21927051@zju.edu.cn (W.L.); zwh114@zju.edu.cn (W.Z.)
[3] Vehicle Engineering Center-CAE Technology Development, Geely Automobile Research Institute, Ningbo 315336, China; colinliao027@163.com
* Correspondence: xucangsu@zju.edu.cn

Abstract: Since both ethanol and acetone are the main components in many alternative fuels, research on the burning characteristics of ethanol-acetone blends is important to understand the combustion phenomena of these alternative fuels. In the present study, the burning characteristics of ethanol-acetone fuel blends are investigated at a temperature of 358 K and pressure of 0.1 MPa with equivalence ratios ranging from 0.7 to 1.4. Ethanol at 100% vol., 25% vol. ethanol/75% vol. acetone, 50% vol. ethanol/50% vol. acetone, 75% vol. ethanol/25% vol. acetone, and 100% vol. acetone are studied by the constant volume combustion chamber (CVCC) method. The results show that the laminar burning velocities of the fuel blends are between that of 100% vol. acetone and 100% vol. ethanol. As the ethanol content increases, the laminar burning velocities of the mixed fuels increase. Furthermore, a detailed chemical kinetic mechanism (AramcoMech 3.0) is used for simulating the burning characteristics of the mixtures. The directed relation graph (DRG), DRG with error propagation (DRGEP), sensitivity analysis (SA), and full species sensitivity analysis (FSSA) are used for mechanism reduction. The flame structure of the skeletal mechanism does not change significantly, and the concentration of each species remains basically the same value after the reaction. The numbers of reactions and species are reduced by 90% compared to the detailed mechanism. Sensitivity and reaction pathway analyses of the burning characteristics of the mixtures indicate that the reaction C_2H_2+H(+M)<=>C_2H_3(+M) is the key reaction.

Keywords: ethanol; acetone; spherically expanding flame; laminar burning characteristics; skeletal mechanism

Citation: Liu, Y.; Liu, W.; Liao, H.; Zhou, W.; Xu, C. An Experimental and Kinetic Modelling Study on Laminar Premixed Flame Characteristics of Ethanol/Acetone Mixtures. *Energies* **2021**, *14*, 6713. https://doi.org/10.3390/en14206713

Academic Editor: Andrea De Pascale

Received: 25 September 2021
Accepted: 12 October 2021
Published: 15 October 2021

1. Introduction

With the rapid development of the automotive industry, increasing numbers of gasoline and diesel vehicles have produced serious air pollution worldwide [1,2]. Besides that, energy shortages in many countries have also attracted researchers' attention in relation to renewable and sustainable energy [3]. Therefore, it is urgent to find efficient and clean alternative fuels, such as bioethanol [4–6], methanol [7–10], dimethyl ether [11], and acetone-butanol-ethanol (ABE) [12–14]. In many alternative fuels, ethanol and acetone are the main components [15,16], so their fundamental combustion characteristics should be well known for their application in gasoline and diesel engines and other burning apparatus. However, there are few studies on the fuel blends of ethanol and acetone. In fact, the fundamental combustion of acetone and ethanol has been studied separately in the literature. Moreover, some studies have investigated the combustion characteristics of ethanol and acetone blends with other fuel. Table 1 lists some research relating to the fundamental combustion characteristics of ethanol, acetone, and ethanol/acetone/other fuel blends.

In this research regarding the fundamental combustion characteristics of alternative fuels, Bradley et al. [17] measured the laminar burning velocities and Markstein numbers of

ethanol/air mixtures at elevated temperatures of 300–393 K and pressures of 0.1–1.4 MPa. The results show that the Markstein number increases slightly when the temperature of the experiment increases and reduces when the pressure of the experiment improves. Broustail et al. [18] provided laminar burning velocity data for ethanol at the initial pressure and temperature of 0.1 MPa and 400 K using the constant volume combustion chamber method. They found that the laminar flame speed of ethanol is higher than that of iso-octane and butanol. Using ethanol in a direct injection engine can effectively prevent knocking. For this reason, Broustail et al. [19] studied the fuel of ethanol and iso-octane. They concluded that the addition of ethanol increases the laminar burning velocity of iso-octane. Moreover, the burning velocity of the fuel blend increases linearly with the increase in ethanol fraction. Dirrenberger et al. [20] measured the laminar burning velocity of gasoline with the addition of ethanol. They observed that the addition of 15% (vol.) ethanol to the mixture has no obvious impact on the laminar burning velocities of gasoline. Varea et al. [21] studied the pressure effects on the laminar burning velocities of ethanol-air mixtures. They verified the reliability of the mechanism for predicting the laminar burning velocity of ethanol and showed that increased pressure causes larger measuring error due to flame cellularity, which occurs on the flame front. Nilsson et al. [22] assessed the laminar burning velocities of acetone/air at room and elevated temperatures. The results show that there is an exponential relationship between laminar burning velocities and temperature. Burluka et al. [23] used the Konnov mechanism to compute the laminar burning velocity and ignition delay of acetone at atmospheric pressure. They noted that acetone/air flames are slow compared with its two isomers, propylene oxide and propionaldehyde. Pichon et al. [24] developed a detailed chemical kinetic model for the oxidation of acetone. They demonstrated that when the addition of acetone is less than 15% by volume, it has no effect on the ignition delay time of an *n*-heptane stoichiometric mixture. Again, Xu et al. [25] studied the laminar burning velocity and flame stability of biomass pyrolysis oil, containing more than 50% ethanol and acetone. They found that it shows good power and emission performance on gasoline and diesel engines. Zhang et al. [26] investigated the laminar premixed flames of ABE (ethanol and acetone content of 47% by volume). Ethanol [27] and acetone [28] were also used as oxygenated fuels in a homogenous charge compression ignition (HCCI) engine. As important components of alternative fuels, there is currently little research on the combustion characteristics of ethanol and acetone fuel blends. Homayoun et al. [29] conducted the vibro-acoustic analysis of a single cylinder. They found that experimental and numerical modal analysis results were in good agreement. These particular mixtures in the special ratios are refined pyrolysis biomass liquid fuels produced by Zhejiang University, which are used in compression-ignition and spark-ignition engines, and they have shown comparable and better emissions than diesel and gasoline.

In order to grasp the heat releasing law and flow field structure in the engine combustion process, and to better design the engine and control the reaction pathways of pollutants, the role of numerical calculation is becoming increasingly important. However, the detailed mechanism containing many components and elementary reactions brings great challenges to numerical calculations. The huge mechanism brings a high degree of nonlinearity and multi-scale, which not only affects the convergence speed of the overall calculation process, but also easily leads to divergence of the solution. In numerical calculation research, it may not be necessary to accurately predict the reaction mechanism in a very wide range, or to pay attention to those components with a mass fraction of less than 10^{-5} [30]. Therefore, the reduction of the mechanism becomes very necessary. It is also a very important research field today. As a starting mechanism, AramcoMech 3.0 [31] is used in this work. AramcoMech 3.0 is based on AramcoMech 2.0 and AramcoMech 1.3. It has been developed to characterize the kinetic and thermochemical properties of a large number of C_1–C_4 hydrocarbons and oxygenated fuels over a wide range of experimental conditions. The methods of directed relation graph (DRG), DRG with error propagation (DRGEP), sensitivity analysis (SA), and full species sensitivity analysis (FSSA) were used

to reduce or simplify the detailed AramcoMech 3.0 [31]. Skeletal mechanisms of fuels with different mixing ratios (ET (100% vol. ethanol), ETAC31 (75% vol. ethanol/25% vol. acetone), ETAC11 (50% vol. ethanol/50% vol. acetone), ETAC13 (25% vol. ethanol/75% vol. acetone), AC (100% vol. acetone)) were used to obtain the burning velocity and compared with the detailed mechanism. What is more, the numerical burning velocity calculated by CHEMKIN was compared with experimental data. Herein, sensitivity and reaction pathway investigations of the tested fuels were also performed.

Table 1. Research on combustion characteristics of ethanol and acetone fuels.

Researchers	Temperature	Pressure	Equivalence Ratio	Method	Fuel
Drenberger et al. [20]	258, 358, 398 K	1 atm	0.5–1.6	HF	ethanol
Sileghem et al. [32]	298–358 K	1 atm	0.7–1.5	HF	ethanol
Rau et al. [33]	298, 323, 348, 373 K	1 atm	0.7–1.4	HF	ethanol
Broustail et al. [19]	423 K	0.1–1.0 MPa	0.7–1.4	CVCC	ethanol
Chong et al. [34]	298 K	1 atm	0.6–1.4	SF	acetone
Nilsson et al. [22]	298, 318, 338, 358 K	1 atm	0.6–1.4	HF	acetone
Gong et al. [35]	343, 393 K	1 atm	0.7–1.6	CVCC	acetone
Wu et al. [36]	375–523 K	0.1–1.0 MPa	0.6–1.3	BF	acetone
Zhang et al. [26]	363 K	30 Torr	1.0	MBMS	ABE
Zhang et al. [37]	358, 393, 428 K	0.1, 0.2, 0.4 MPa	0.7–1.5	CVCC	ABE
Zhang et al. [38]	400 K	0.1 MPa	0.6–1.6	CVCC	ABE

HF, heat flux; CVCC, constant volume combustion chamber; SF, stagnation flame; BF, Bunsen flame; MBMS, molecular beam mass spectrometry.

Ethanol-acetone fuel blends have been used in combustion engines and industry; however, there is no literature in relation to these. In this work, the laminar burning characteristics of ethanol-acetone fuel blends were studied at a temperature of 358 K and pressure of 0.1 MPa with equivalence ratios ranging from 0.7 to 1.4. The laminar burning velocities, sensitivity analysis, reaction path, and flame structure of different ratios of ethanol-acetone fuel blends were investigated. The methods of directed relation graph (DRG), DRG with error propagation (DRGEP), sensitivity analysis (SA), and full species sensitivity analysis (FSSA) were used to calculate and analyze kinetic modelling based on AramcoMech 3.0.

2. Experimental and Computational Methods

The experimental system is based on a constant volume combustion chamber, while computational methods used in this study are directed relation graph (DRG), DRG with error propagation (DRGEP), sensitivity analysis (SA), and full species sensitivity analysis (FSSA) with CHEMKIN software.

2.1. Experimental Device

Figure 1 shows the image of the experimental system and the experimental device. The experimental system includes a constant volume combustion chamber, an ignition system, and a high-speed Schlieren photography system. The front and rear surfaces of the constant volume bomb (200 × 200 × 200 mm) are equipped with quartz glass windows (105 mm) for optical detection. The left and right surfaces are equipped with central electrode mounting holes for igniting the mixture. The upper surface is equipped with intake and exhaust holes, an installed pressure sensor (Kistler 6155B), and a thermocouple (WRNK-234). In addition, heating resistors are evenly arranged on each surface of the constant volume bomb to control the initial temperature of the experiment. The Z-shape Schlieren system is connected with a high-speed camera to obtain the flame images. The high-speed camera used in the experiment was a Photron FASTCAM. Figure 1b shows the constant volume combustion chamber used in the system. More information on the experimental apparatus can be found in the previous papers [25,39–42].

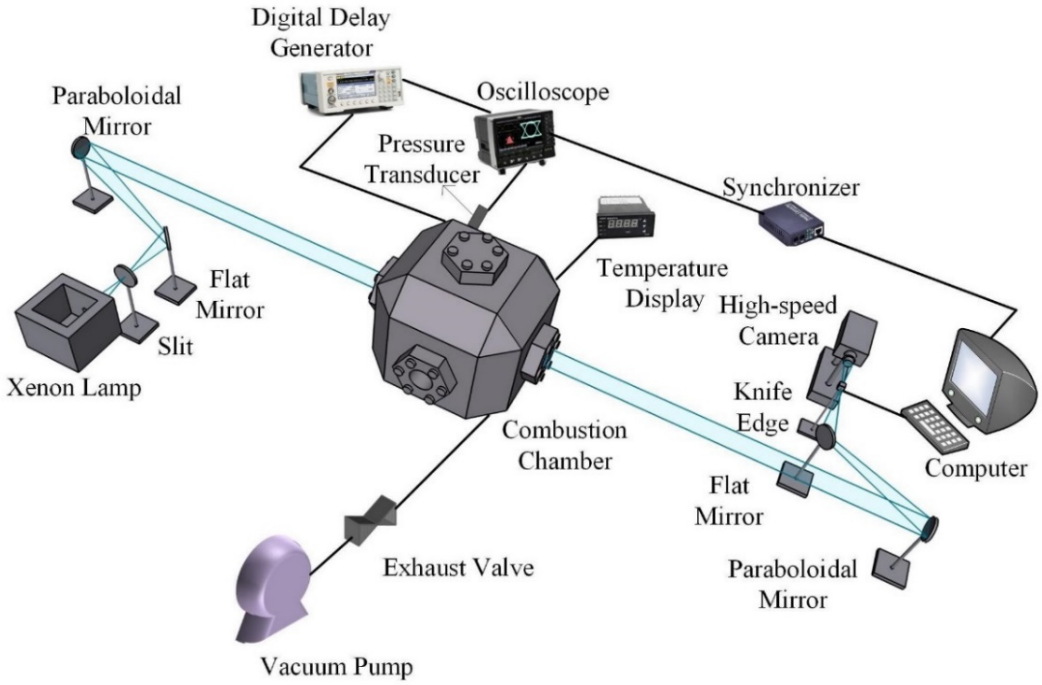

(**a**)

(**b**)

Figure 1. The experimental system (**a**) and the experimental device (**b**).

2.2. Data Processing

Matlab was used to obtain the flame radius. The radius of the flame r_f can be obtained as [43]:

$$r_f = \sqrt{\frac{S_f}{S_a}} R_0 \tag{1}$$

where S_f is the flame surface-surrounded pixels, S_a is the total pixel points contained in the window, and R_0 is the actual radius of the window. The value of R_0 is 52.5 mm. After obtaining the flame radius, the stretched flame propagation speed is calculated using Equation (2) [25]:

$$S_b = \frac{dr_f}{dt} \tag{2}$$

where S_b is the stretched laminar flame speed and t is the time after ignition. By calculating the stretched laminar flame speed, the flame stretch rate (κ) was calculated by [39]:

$$\kappa = 2\frac{S_b}{r_f} \tag{3}$$

The flame stretch rate, κ, is defined as the logarithm of an infinitely small area of the flame surface versus time. Then, the nonlinear correlation of unstretched laminar flame speed and stretched laminar flame speed were calculated. The correlation between unstretched laminar flame speed S_b^0 and stretched laminar flame speed S_b are given as [21]:

$$\left(\frac{S_b}{S_b^0}\right)^2 ln\left(\frac{S_b}{S_b^0}\right)^2 = -\frac{L_b}{S_b^0}\kappa \tag{4}$$

where L_b is Markstein length. According to the mass conservation theory, the laminar burning velocity u_L can be obtained as follows [40]:

$$\rho_u u_L = \rho_b S_b^0 \tag{5}$$

where ρ_u and ρ_b are the density of the burned gas and unburned gas under the isobaric assumption, which are calculated by the Chemkin software.

2.3. Uncertainty Assessment

The uncertainty of laminar burning velocity is mainly caused by measurement repeatability and thermal radiation. The uncertainty caused by measurement repeatability belongs to type A uncertainty. Each set of experiments in this study was repeated three times, and the standard deviations R_1 were calculated. According to previous studies, the influence of thermal radiation on the laminar burning velocity mainly lies in two aspects: one is that the thermal radiation of the flame will directly reduce the temperature of the flame; the other is that the radiant cooling causes the fuel gas to flow inward. Both of these influence modes cause the flame propagation speed to decrease. Yu et al. [44] proposed an empirical formula for calculating the uncertainty of laminar burning velocity (R_2) caused by thermal radiation:

$$R_2 = 0.82 \times \left(\frac{u_L}{S_0}\right)^{-1.14}\left(\frac{T}{T_0}\right)\left(\frac{p}{p_0}\right)^{-0.3} \tag{6}$$

where S_0 is 1 cm·s^{-1}, T_0 is 298 K, p_0 is 1 atm, u_L is laminar burning velocity, T is the temperature of the bomb, p is the pressure of the bomb, and R_2 is the uncertainty of laminar burning velocity caused by radiation. This empirical formula is used in the constant volume bomb method for determining the uncertainty of the laminar flame velocity. Therefore, the uncertainty of laminar burning velocity (R) was calculated by [41]:

$$R = \sqrt{R_1^2 + R_2^2} \tag{7}$$

The uncertainty of laminar burning velocity (R) was less than 5.92% in this work.

3. Results and Discussion

Firstly, the experimental system was validated by the laminar burning velocities of ethanol. Then the mechanism reduction was processed and the skeletal mechanism was obtained. The laminar burning velocities of the experiment and the simulation were compared. Finally, sensitivity, reaction pathways, and flame structures were analyzed.

3.1. System Validation

Figure 2 compares the laminar burning velocities of ethanol in the literature and this work at a temperature of 358 K and a pressure of 0.1 MPa. It can be seen from the figure that the data from this work and the literature [17,20,45] are consistent and agree well with each other. On the lean side, the data from this work are somehow comparable with data from Bradley et al. [17]; the deviation is less than 6%. Meanwhile, on the rich side, they are somewhat comparable with Dirrenberger et al. [20]; the deviation is less than 12%. In view of the above discussion, the experimental setup of this work is very reliable.

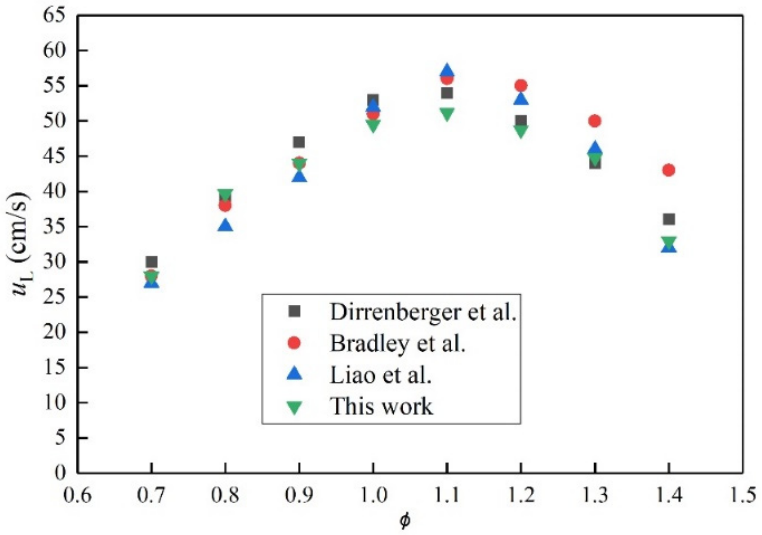

Figure 2. Comparison of u_L of ethanol in this work and other researchers' results.

3.2. Mechanism Reduction

Chemkin is thermochemical object-oriented software used for solving thermodynamic, kinetic, and transport process problems. It can be used to investigate combustion, detonation, electrochemical energy conversion and storage problems, and the like. It has objects which represent phases of matter, time-independent reactors, steady one-dimensional reacting flows, etc. Besides, Chemkin can be used to analyze flame problems such as the freely-propagating premixed laminar flame, burner flame, counter flow premixed and diffusion flame, ion free flame, etc. in one-dimensional reacting flow problems. The freely-propagating flame is used in this work to investigate the burning velocity of ethanol-acetone fuels. In this study, the premixed laminar burning velocity module of Chemkin software was used for the simulations, in the area of 1 cm, with a maximum grid point of 1000 (GRAD = 0.1, GURV = 0.5). Various methods such as DRG, DRGEP, SA, and FSSA were combined to simplify the detailed mechanism. Generally, the detailed mechanism of these several fuels goes through a three-step reduction process, as shown in Figure 3. DRGEP and DRG have the same basic principle. In this research, DRG or DRGEP were initially used to reduce the detailed mechanism, because DRG and DRGEP were used to check the coupling relationship between components and to remove unimportant species. Then, the results of DRG and DRGEP (Skeletal Mechanism #1(DRG) and Skeletal Mechanism #1(DRGEP), respectively) were compared to determine the mechanism with fewer species and reactions as the result of the first-step reduction (Skeletal Mechanism #1). Sensitivity analysis for a group of substances by DRGSA and DRGEPSA optimized Skeletal Mechanism #1 to Skeletal Mechanism #2(DRGSA) and Skeletal Mechanism #2(DRGEPSA), respectively. As for the first step, the simplified results of the two methods were compared, and the mechanism with lower results was chosen as Skeletal Mechanism #2. Finally, components in Skeletal Mechanism #2 were further reduced by FSSA to obtain Skeletal Mechanism #3.

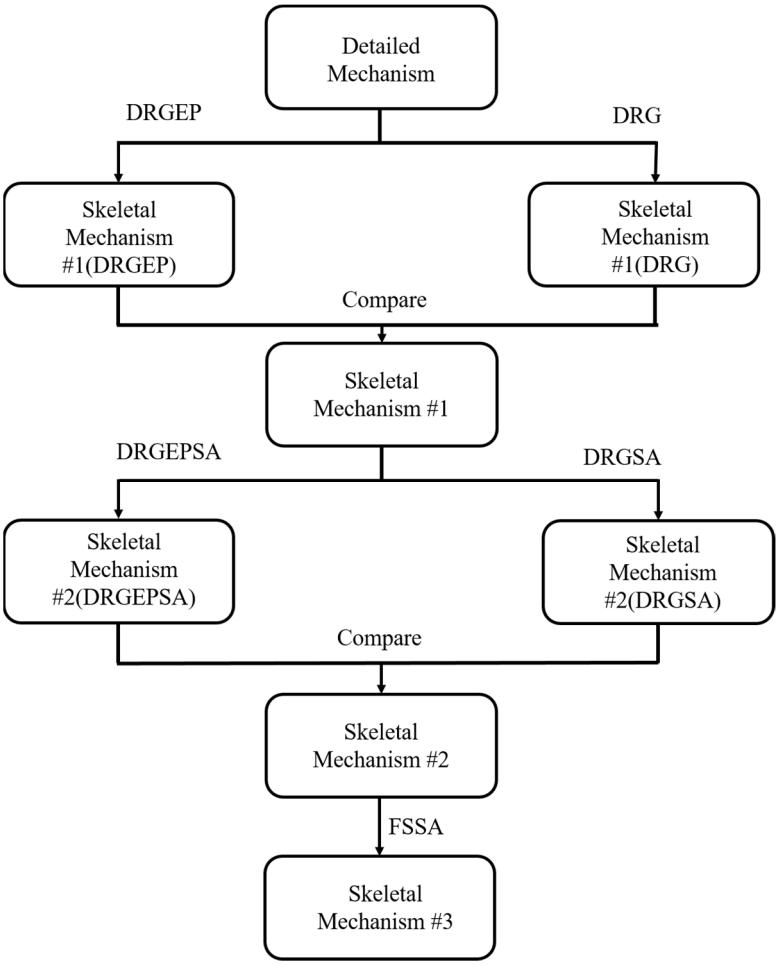

Figure 3. Mechanism reduction process.

Two target parameters were set as key criteria in the process, including acetylene (C_2H_2) concentration and carbon monoxide (CO) concentration [46]. There are several reasons for this set. C_2H_2 can characterize the intermediate products of soot [47]. The combustion of fuels may form the common intermediate of C_2H_2, which may undergo simultaneous polymerization and dehydrogenation to produce long-chain polyacetylene and finally convert into soot [48]. Under high-temperature conditions, CO, CO_2, and O_2 maintain a certain balance. CO is the main exothermic reactant in the high-temperature oxidation stage. Therefore, the concentrations of C_2H_2 and CO were set as key species in reducing the mechanism. The process is shown in Table 2.

Table 2. Methods used in the mechanism reduction process and number of species/reactions after each step (the detailed mechanism includes 581 species and 3037 reactions).

Step	ET	ETAC31	ETAC11	ETAC13	AC
1	DRG 111/740	DRGEP 87/493	DRGEP 123/854	DRGEP 117/759	DRGEP 119/825
2	DRGEPSA 64/383	DRGSA 82/468	DRGSA 65/385	DRGSA 70/387	DRGSA 94/618
3	FSSA 44/270	FSSA 66/398	FSSA 54/327	FSSA 65/330	FSSA 47/274

Previous studies showed that free radicals are the most important elementary substances in the reactions [49], especially the hydroxyl radical (OH), which has a great influence on the process of combustion. Figure 4 compares the simulated mole fraction results of OH by the detailed mechanism and skeletal mechanism of the fuel at a temperature of 358 K and a pressure of 1 atm. Both detailed mechanism and skeletal mechanism predict the peak OH mole fraction at ϕ = 1.0. Compared with the detailed mechanism, the average relative deviation of the skeletal mechanism for ethanol is 1.7% (ET), while that for acetone is only 1.2% (AC).

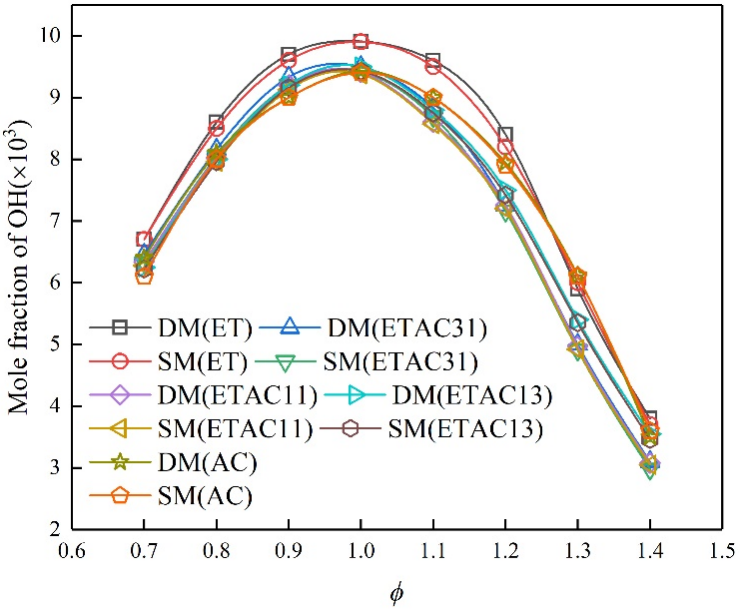

Figure 4. Comparison of OH mole fraction calculated by skeletal mechanism and detailed mechanism. DM: detailed mechanism; SM: skeletal mechanism.

Figure 5 displays mole fraction profiles of CO_2 computed with the skeletal mechanism and detailed mechanism. The results show that the peak values are attained at ϕ = 0.9. The average relative deviation is less than 0.5%. In view of the above discussion, the skeletal mechanisms of acetone and ethanol are reliable.

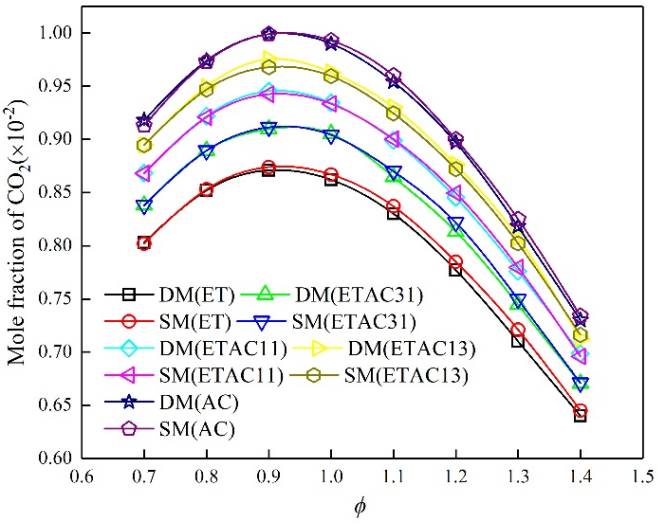

Figure 5. Comparison of CO_2 mole fraction calculated by skeletal mechanism and detailed mechanism. DM: detailed mechanism; SM: skeletal mechanism.

3.3. Laminar Burning Velocity

Figure 6 shows the flame images of ETAC11 at ϕ = 0.8, 1.0, 1.1, and 1.3, with an initial temperature of 358 K and pressure of 0.1 MPa. The flame speed is highest at the stoichiometric equivalence ratio, ϕ = 1.0. The decrease in the flame speed at the lean side (ϕ = 0.8) is more pronounced than that at the rich side (ϕ = 1.3).

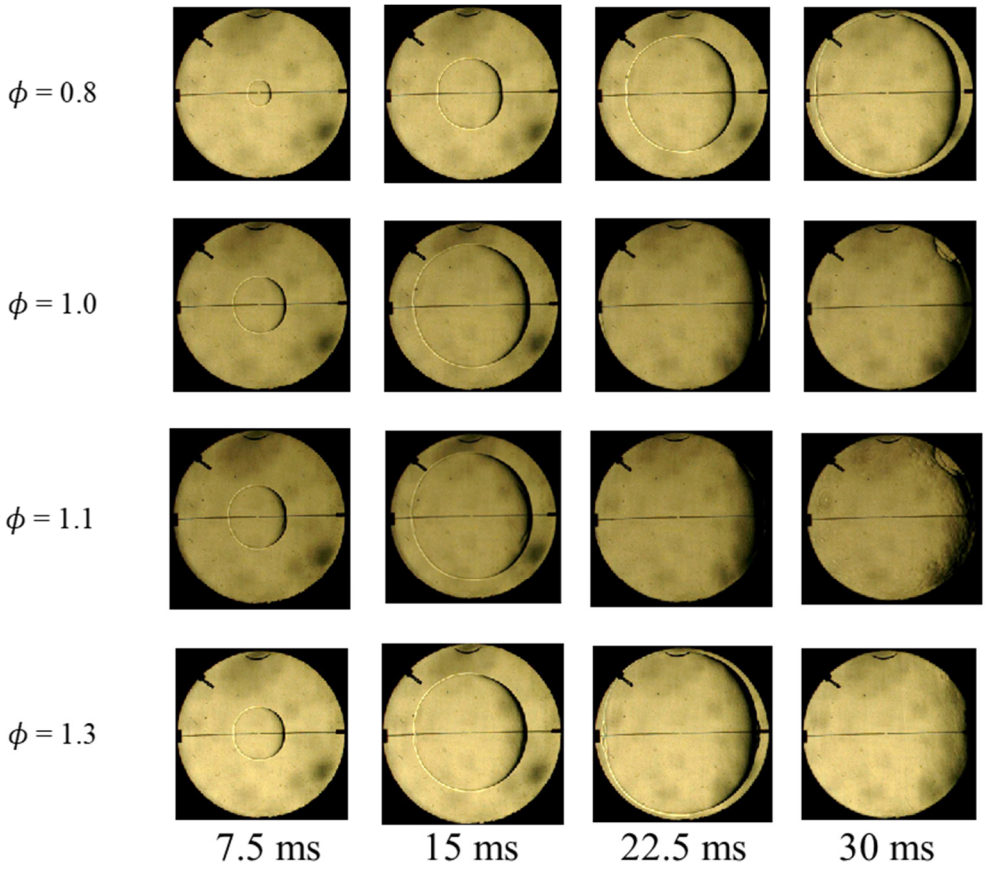

Figure 6. Flame images of ETAC11 (50% ethanol + 50% acetone by volume) at different equivalence ratios, with an initial temperature of 358 K and pressure of 0.1 MPa.

Figure 7 shows the laminar burning velocities of ethanol and acetone. The laminar burning velocities of ethanol and acetone reached a maximum value of u_L = 50.1 cm/s and u_L = 43 cm/s at ϕ = 1.1 and 1.0, respectively. The results simulated by the skeletal mechanism are close to the experimental data. The simulation results of acetone fit the experimental data better on the lean fuel side. The simulation and experimental data are consistent in trend; however, the relative difference between the simulation and the experimental data is 21% for acetone and 12.6% for ethanol. As the ethanol content increases, the laminar burning velocities of the mixed fuels increase. 1-hydroxyethyl (SC_2H_4OH) and 2-hydroxyethyl (PC_2H_4OH) are two active radicals generated by ethanol, which can easily produce OH during the combustion process. OH (hydroxyl) is an active radical that has a significant effect on the laminar burning velocity. The increase in ethanol content raises the fraction of OH, which renders the laminar burning velocity larger. The flame speed of the fuel blend reaches a maximum at ϕ = 1.0~1.1. The difference between experimental data and simulation results for ethanol on the fuel-lean side are smaller than that on the fuel-rich side, with 10% and 15%, respectively. Laminar burning velocities of the fuel blend is between those of acetone and ethanol. A flame speed model was used to calculate with the skeletal mechanism and the detailed mechanism. Such a model is different from homogeneous mixtures in a closed bomb of the experiment in that the radical concentration in the flame of the flame speed model is always higher than that

generated during the induction period of homogeneous ignition. Besides that, in the flame environment of the flame speed model, steep temperature and concentration gradients exist, which can bring radicals produced in the high-temperature region of the flame to a low-temperature region, thereby facilitating the reactions causing results of simulation that are higher than those of the experiment [46]. The laminar burning velocities simulated by the detailed mechanism are higher than those by the skeletal mechanism, due to the reduction of formation of OH in the mechanism reduction process. In order to simplify the detailed mechanism, the number of radicals was decreased in the calculation process, which reduced the formation of OH. The average deviation of the skeletal mechanism and experimental data is around 20%, while the average deviation of the detailed mechanism and experimental data is about 35%. The reason for the deviation is that the radiation effect is not considered in skeletal and detailed mechanisms, and it renders the over-predictions of laminar burning velocities.

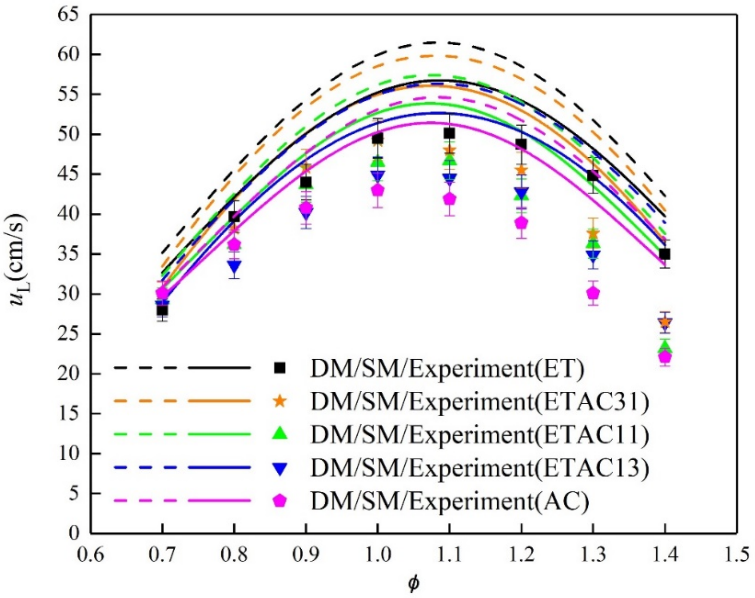

Figure 7. Experimental and numerical laminar burning velocities of the fuel blend of ethanol and acetone at an initial temperature of 358 K and pressure of 0.1 MPa.

Sarli et al. [50] investigated a Le Chatelier's rule formula that is based on the mole fraction for the laminar burning velocity of fuel mixtures, and they calculated a good prediction in lean and stoichiometric regions. The equation is expressed as:

$$u_{L,blend} = \frac{1}{\sum_{i=1}^{n} \frac{x_i}{u_{L,i}}} \quad (8)$$

where x_i is the mole fraction of each component, $u_{L,blend}$ is the laminar burning velocity of fuel mixtures, and $u_{L,i}$ is the laminar burning velocity of pure fuel. Figure 8 shows the comparison between estimated results calculated by Le Chatelier's rule and experimental data of ETAC11. The deviation of the two calculation results is less than 15%

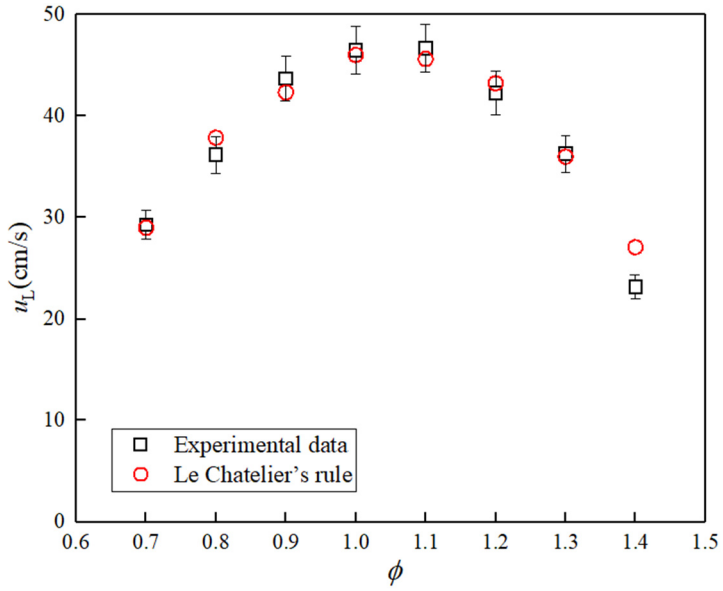

Figure 8. The comparison between estimated results calculated by Le Chatelier's rule and experimental data of ETAC11.

3.4. Sensitivity Analysis and Reaction Path

The reaction pathways of ethanol and acetone were also simulated with the skeletal mechanism. Figure 9 shows the top ten reactions with the highest sensitivity coefficients of the three fuel blends to analyze sensitivity at 50% fuel consumption. In this work, C_2H_2+H(+M)<=>C_2H_3(+M) has a clear consumption effect on ethanol and acetone of the mixtures, which means it leads to advancing effects on the laminar burning velocities. Besides that, C_2H_4 is the significant substance that increases the laminar burning velocities. In addition, at $\phi = 1.0$, the main consumption of ethanol comes from H abstraction reactions, while the main acetone consumption is the decomposition of CH_3CO. CO oxidation inhibits consumption of both acetone and ethanol.

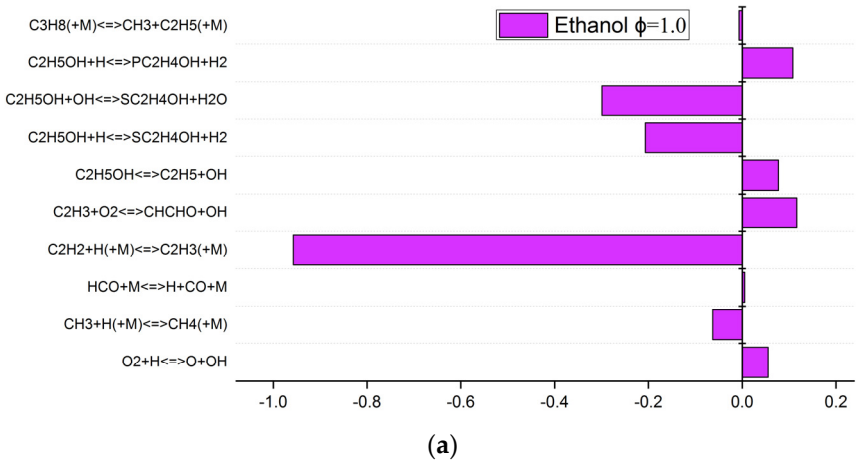

(**a**)

Figure 9. *Cont.*

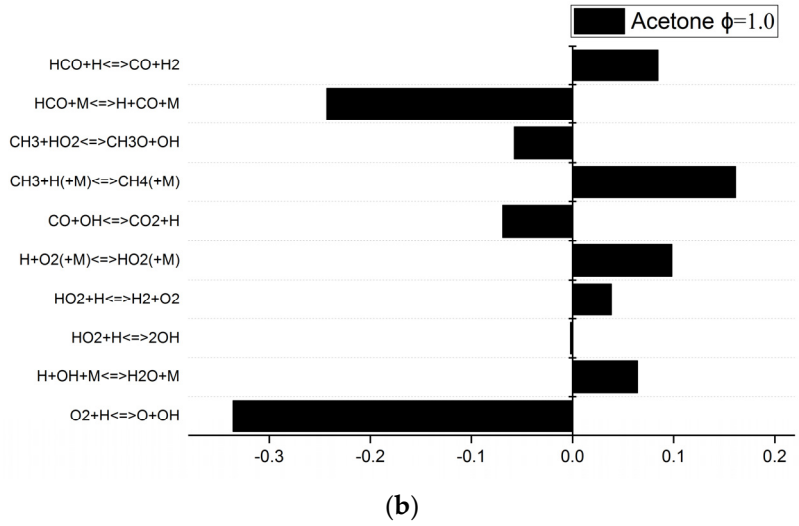

(**b**)

Figure 9. Sensitivity analyses of mixed fuel ETAC31 at $\phi = 1.0$ ((**a**) ethanol, (**b**) acetone).

Figure 10 demonstrates the main reaction pathways of ethanol and acetone of ETAC11 fuel at 50% fuel consumption calculated by the detailed mechanism and the skeletal mechanism. In this work, ethanol generates two active free radicals (1-hydroxyethyl, SC_2H_4OH and 2-hydroxyethyl, PC_2H_4OH) through H-abstraction, and then produces an important intermediate product, acetaldehyde (CH_3CHO). Tsang et al. [51] considered six ways of ethanol decomposition and showed that the elimination of water, $C_2H_5OH(+M) = C_2H_4 + H_2O(+M)$, is the most important pathway. The two reaction pathways of ethanol leading to SC_2H_4OH and PC_2H_4OH in the initial stage of the combustion of ethanol in this work account for more than 95% of its consumption, and other pathways were removed. Tran et al. [52] set ethylene (C_2H_4) as a significant intermediate in the combustion of ethanol, the same as the results in this work. Li et al. [53] divided the decomposition of acetone into two pathways ($CH_3CO + CH_3/CH_3COCH_2$). In this work, the pathway leading to 1-acetonyl (CH_3COCH_2) was determined to be the main pathway. Compared with the detailed mechanism, some unimportant chain reactions in the skeletal mechanism are removed. In reaction pathways of ethanol, C2H5O is eliminated, which accounts for 1.45% of ethanol decomposition in the detailed mechanism, while some species such as IC_3H_7O and $C_3H_6OH_2$-1 are removed by acetone reaction pathways in the detailed mechanism.

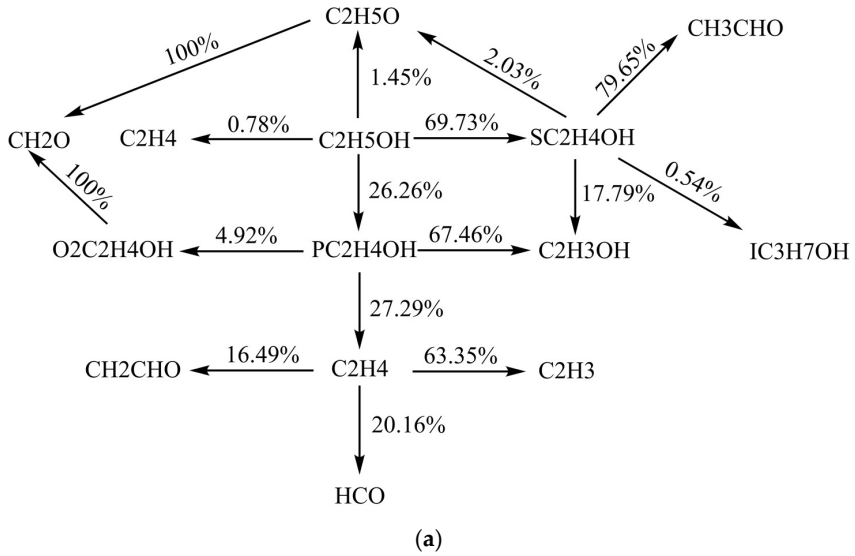

(**a**)

Figure 10. *Cont.*

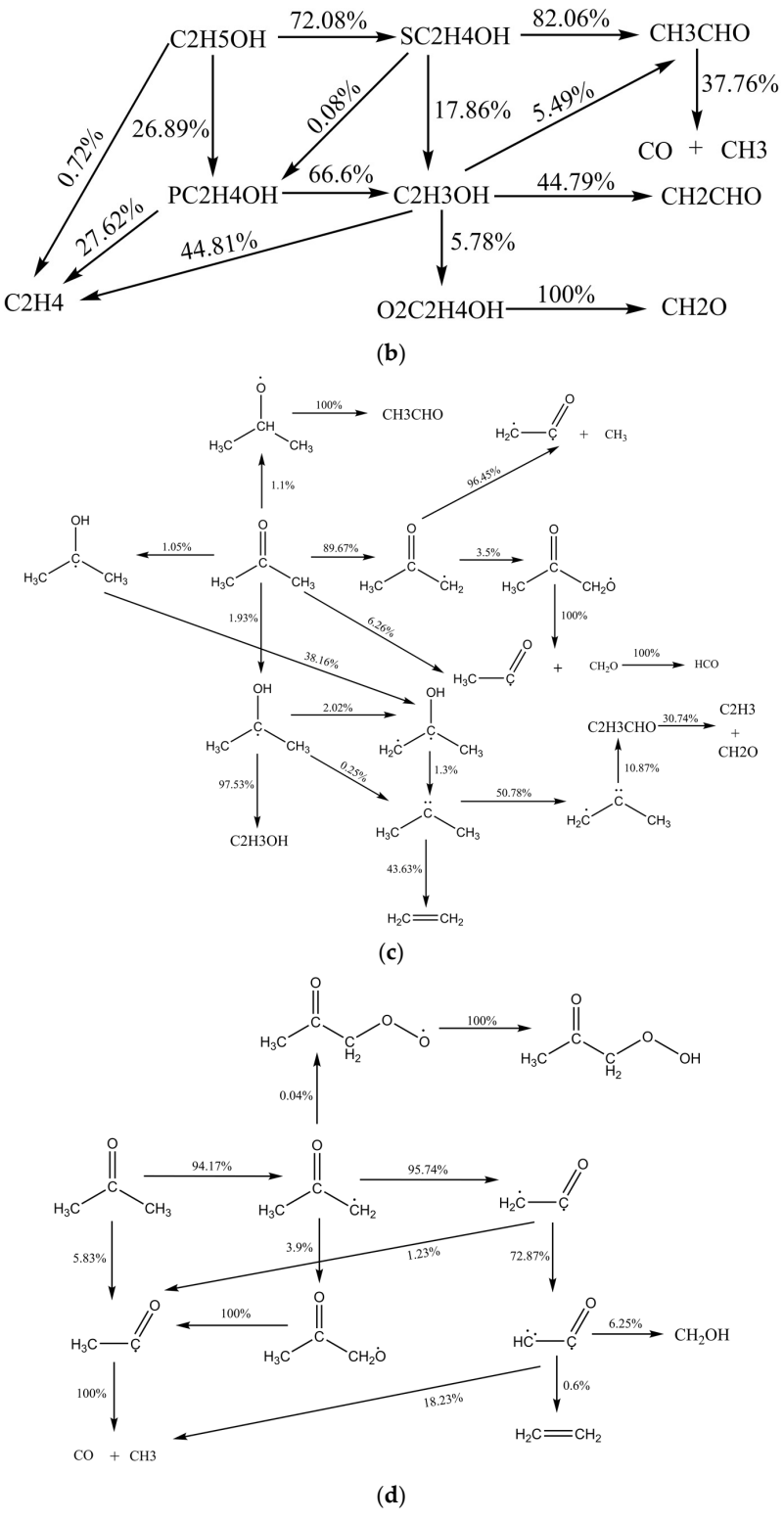

Figure 10. The main reaction paths of ethanol and acetone of ETAC11 at the equivalence ratio of 1.0 ((**a**) ethanol, detailed mechanism, (**b**) ethanol, skeletal mechanism, (**c**) acetone, detailed mechanism, (**d**) acetone, skeletal mechanism).

Figure 11 illustrates the flame structure of ETAC11 at the equivalence ratio of 1.0. By comparing the concentration of each species in the two mechanisms, the flame structure of the skeletal mechanism did not change significantly, and the concentration of each species remained basically the same value after the reaction. In the calculation results of the detailed mechanism, the combustion reaction position is around 1 cm, while the reaction position of the detailed mechanism is around 0.2 cm.

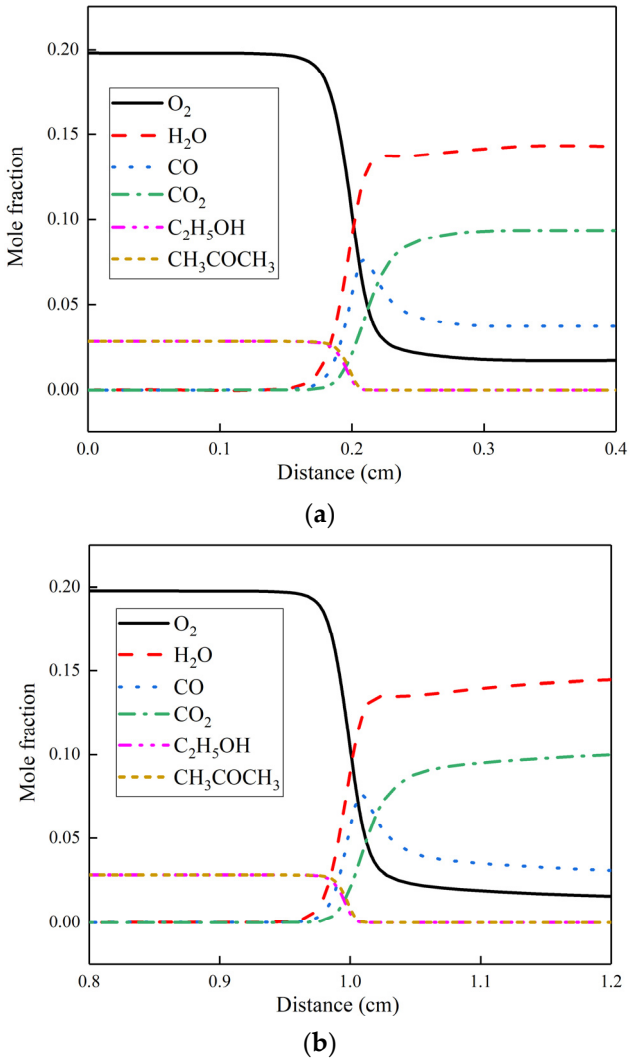

Figure 11. The flame structure at the equivalence ratio of 1.0 of ETAC11 ((**a**) detailed mechanism, (**b**) skeletal mechanism).

4. Conclusions

This work investigated the laminar burning velocities of 5 different fuels at T_0 = 358 K and p_0 = 0.1 MPa in a constant volume combustion chamber with equivalence ratios ranging from 0.7 to 1.4. Numerical calculations of the laminar burning velocities were also studied in this work, and DRG, DRGEP, SA, and FSSA were used to reduce the detailed mechanism. Furthermore, the sensitivity and path of the reactions were analyzed for mixed fuels. The main conclusions are summarized as follows. This is the first time that ethanol/acetone mixtures have been investigated concerning their burning velocities. Besides that, the novelty of the present work is studying the mechanism of reduction of ethanol/acetone mixtures first.

- Compared with pure fuel, the laminar burning velocity of mixed fuel is lower than that of ethanol and higher than the laminar burning velocity of acetone. The laminar burning velocity increases with increasing ethanol content.
- Through a three-step reduction process, the best simplification method is selected for each step and species, and the number of reactions of the detailed mechanism have been reduced by 90%.
- Multiple reduction methods were combined to alternately simplify the detailed mechanisms to skeletal mechanisms that are suitable for different mixed fuels. The calculation results of the skeletal mechanisms and the experimental results have similar trends.
- C_2H_2+H(+M)<=>C_2H_3(+M) has a clear consumption effect on ethanol and acetone of the mixtures, which means it leads to advancing effects on the laminar burning velocities.
- The flame structure of the skeletal mechanism did not change significantly, and the concentration of each species remained basically the same value after the reaction.

Author Contributions: Conceptualization and writing—original draft preparation, Y.L. and W.L.; methodology, H.L.; software, W.L.; validation, W.Z.; funding acquisition, C.X. and Y.L. All authors have read and agreed to the published version of the manuscript.

Funding: This research received no external funding.

Institutional Review Board Statement: Not applicable.

Informed Consent Statement: Not applicable.

Acknowledgments: The authors are indebted to Basic Scientific Research Project of Zhejiang Technical Institute of Economics (JKY2021014), and the National Key R&D Program of China (2018YFB1501405) for funding this work.

Conflicts of Interest: The authors declare that they have no known competing financial interests or personal relations.

Nomenclature

CVCC	Constant volume combustion chamber
DRG	Directed relation graph
DRGEP	DRG with error propagation
SA	Sensitivity analysis
FSSA	Full species sensitivity analysis
HF	Heat flux
SF	Stagnation flame
BF	Bunsen flame
L_b	Markstein length
ρ_{u}	Density of unburned gas
$\boldsymbol{R}$	Uncertainty of laminar burning velocity
R_2	Uncertainty of laminar burning velocity caused by radiation
$\boldsymbol{p}$	Pressure of bomb
SM	Skeletal mechanism
ETAC11	50% vol. ethanol/50% vol. acetone
ETAC31	75% vol. ethanol/25% vol. acetone
MBMS	Molecular beam mass spectrometry
r_f	Radius of the flame
S_f	Flame surface-surrounded pixels

S_a	Total pixel points contained in the window
R_0	Actual radius of the window
S_b	Stretched laminar flame speed
κ	Flame stretch rate
S_b^0	Unstretched laminar flame speed
ρ_b	Density of burned gas
u_L	Laminar burning velocity
R_1	Standard deviations of experiment
$\boldsymbol{T}$	Temperature of bomb
DM	Detailed mechanism
ET	100% vol. ethanol
ETAC13	25% vol. ethanol/75% vol. acetone
AC	100% vol. acetone

References

1. Kontses, A.; Triantafyllopoulos, G.; Ntziachristos, L.; Samaras, Z. Particle number (PN) emissions from gasoline, diesel, L.P.G., C.N.G and hybrid-electric light-duty vehicles under real-world driving conditions. *Atmos. Environ.* **2020**, *222*, 117126. [CrossRef]
2. Gao, D.; Li, Z.; Liu, P.; Zhao, J.; Zhang, Y.; Li, C. A coordinated energy security model taking strategic petroleum reserve and al-ternative fuels into consideration. *Energy* **2018**, *145*, 171–181. [CrossRef]
3. Kroyan, Y.; Wojcieszyk, M.; Kaario, O.; Larmi, M.; Zenger, K. Modeling the end-use performance of alternative fuels in light-duty vehicles. *Energy* **2020**, *205*, 117854. [CrossRef]
4. Asad, U.; Kumar, R.; Zheng, M.; Tjong, J. Ethanol-fueled low temperature combustion: A pathway to clean and efficient diesel engine cycles. *Appl. Energy* **2015**, *157*, 838–850. [CrossRef]
5. Thangavelu, S.K.; Ahmed, A.S.; Ani, F.N. Review on bioethanol as alternative fuel for spark ignition engines. *Renew. Sustain. Energy Rev.* **2016**, *56*, 820–835. [CrossRef]
6. Compagnoni, M.; Mostafavi, E.; Tripodi, A.; Mahinpey, N.; Rossetti, I. Techno-economic Analysis of a Bioethanol to Hydrogen Centralized Plant. *Energy Fuels* **2017**, *31*, 12988–12996. [CrossRef]
7. Matzen, M.; Demirel, Y. Methanol and dimethyl ether from renewable hydrogen and carbon dioxide: Alternative fuels pro-duction and life-cycle assessment. *J. Clean. Prod.* **2016**, *139*, 1068–1077. [CrossRef]
8. Wei, H.; Yao, C.; Pan, W.; Han, G.; Dou, Z.; Wu, T.; Liu, M.; Wang, B.; Gao, J.; Chen, C.; et al. Experimental investigations of the effects of pilot injection on combustion and gaseous emission characteristics of diesel/methanol dual fuel engine. *Fuel* **2017**, *188*, 427–441. [CrossRef]
9. Anderson, J.E.; Kramer, U.; Mueller, S.A.; Wallington, T.J. Octane Numbers of Ethanol− and Methanol−Gasoline Blends Estimated from Molar Concentrations. *Energy Fuels* **2010**, *24*, 6576–6585. [CrossRef]
10. Vancoillie, J.; Christensen, M.; Nilsson, E.J.K.; Verhelst, S.; Konnov, A.A. Temperature Dependence of the Laminar Burning Veloc-ity of Methanol Flames. *Energy Fuels* **2012**, *26*, 1557–1564. [CrossRef]
11. Park, S.H.; Lee, C.S. Applicability of dimethyl ether (DME) in a compression ignition engine as an alternative fuel. *Energy Convers. Manag.* **2014**, *86*, 848–863. [CrossRef]
12. Wu, H.; Nithyanandan, K.; Zhang, J.; Lin, Y.; Lee, T.H.; Chia-fon, F.L.; Zhang, C. Impacts of Acetone–Butanol–Ethanol (ABE) ratio on spray and combustion characteristics of ABE–diesel blends. *Appl. Energy* **2015**, *149*, 367–378. [CrossRef]
13. Wu, H.; Nithyanandan, K.; Zhou, N.; Lee, T.H.; Lee, C.-F.F.; Zhang, C. Impacts of acetone on the spray combustion of Acetone–Butanol–Ethanol (ABE)-Diesel blends under low ambient temperature. *Fuel* **2015**, *142*, 109–116. [CrossRef]
14. Zhao, Z.; Wu, H.; Wang, M.; Lee, C.-F.; Liu, J.; Fu, J.; Chang, W. Computational Investigation of Oxygen Concentration Effects on a Soot Mechanism with a Phenomenological Soot Model of Acetone–Butanol–Ethanol (ABE). *Energy Fuels* **2015**, *29*, 1710–1721. [CrossRef]
15. Li, Y.; Ning, Z.; Chia-fon, F.L.; Yan, J.; Lee, T.H. Effect of acetone-butanol-ethanol (ABE)–gasoline blends on regulated and unregulat-ed emissions in spark-ignition engine. *Energy* **2019**, *168*, 1157–1167. [CrossRef]
16. Bhowmik, S.; Paul, A.; Panua, R.; Ghosh, S.K. Performance, combustion and emission characteristics of a diesel engine fueled with diesel-kerosene-ethanol: A multi-objective optimization study. *Energy* **2020**, *211*, 118305. [CrossRef]
17. Bradley, D.; Lawes, M.; Mansour, M. Explosion bomb measurements of ethanol–air laminar gaseous flame characteristics at pressures up to 1.4MPa. *Combust. Flame* **2009**, *156*, 1462–1470. [CrossRef]
18. Broustail, G.; Seers, P.; Halter, F.; Moréac, G.; Mounaim-Rousselle, C. Experimental determination of laminar burning velocity for butanol and ethanol iso-octane blends. *Fuel* **2011**, *90*, 1–6. [CrossRef]
19. Broustail, G.; Halter, F.; Seers, P.; Moréac, G.; Mounaïm-Rousselle, C. Experimental determination of laminar burning velocity for butanol/iso-octane and ethanol/iso-octane blends for different initial pressures. *Fuel* **2013**, *106*, 310–317. [CrossRef]
20. Dirrenberger, P.; Glaude, P.; Bounaceur, R.; Le Gall, H.; da Cruz, A.P.; Konnov, A.; Battin-Leclerc, F. Laminar burning velocity of gasolines with addition of ethanol. *Fuel* **2014**, *115*, 162–169. [CrossRef]
21. Varea, E.; Modica, V.; Renou, B.; Boukhalfa, A.M. Pressure effects on laminar burning velocities and Markstein lengths for Iso-octane–Ethanol–Air mixtures. *Proc. Combust. Inst.* **2013**, *34*, 735–744. [CrossRef]

22. Nilsson, E.; de Goey, L.; Konnov, A. Laminar burning velocities of acetone in air at room and elevated temperatures. *Fuel* **2013**, *105*, 496–502. [CrossRef]
23. Burluka, A.A.; Harker, M.; Osman, H.; Sheppard, C.G.W.; Konnov, A.A. Laminar burning velocities of three C3H6O isomers at at-mospheric pressure. *Fuel* **2010**, *89*, 2864–2872. [CrossRef]
24. Pichon, S.; Black, G.; Chaumeix, N.; Yahyaoui, M.; Simmie, J.; Curran, H.; Donohue, R. The combustion chemistry of a fuel tracer: Meas-ured flame speeds and ignition delays and a detailed chemical kinetic model for the oxidation of acetone. *Combust. Flame* **2009**, *156*, 494–504. [CrossRef]
25. Xu, C.; Wang, H.; Oppong, F.; Li, X.; Zhou, K.; Zhou, W.; Wu, S.; Wang, C. Determination of laminar burning characteristics of a surrogate for a pyrolysis fuel using constant volume method. *Energy* **2020**, *190*, 116315. [CrossRef]
26. Zhang, R.; Sun, W.; Tao, T.; Yang, B. Species diagnostics and modeling study of laminar premixed flames fueled by acetone–butanol–ethanol (ABE). *Proc. Combust. Inst.* **2017**, *36*, 1303–1310. [CrossRef]
27. Bendu, H.; Deepak, B.; Murugan, S. Application of G.R.NN for the prediction of performance and exhaust emissions in HCCI engine using ethanol. *Energy Convers. Manag.* **2016**, *122*, 165–173. [CrossRef]
28. Zhang, C.; Wu, H. Combustion characteristics and performance of a methanol fueled homogenous charge compression igni-tion (HCCI) engine. *J. Energy Inst.* **2016**, *89*, 346–353. [CrossRef]
29. Homayoun, M.R.; Moradikazerouni, A. Vibro-acoustic Analysis of a Single Cylinder in Multi-stage Reciprocating Compres-sors. In Proceedings of the 3rd International Conference on Mechanical and Aerospace Engineering, Tehran, Iran, April 2018.
30. Selle, L. Compressible large eddy simulation of turbulent combustion in complex geometry on unstructured meshes. *Combust. Flame* **2004**, *137*, 489–505. [CrossRef]
31. Zhou, C.-W.; Li, Y.; Burke, U.; Banyon, C.; Somers, K.P.; Ding, S.; Khan, S.; Hargis, J.W.; Sikes, T.; Mathieu, O.; et al. An experimental and chemical kinetic modeling study of 1,3-butadiene combustion: Ignition delay time and laminar flame speed measurements. *Combust. Flame* **2018**, *197*, 423–438. [CrossRef]
32. Sileghem, L.; Alekseev, V.A.; Vancoillie, J.; Nilsson, E.J.K.; Verhelst, S.; Konnov, A.A. Laminar burning velocities of primary ref-erence fuels and simple alcohols. *Fuel* **2014**, *115*, 32–40. [CrossRef]
33. Rau, F.; Hartl, S.; Voss, S.; Still, M.; Hasse, C.; Trimis, D. Laminar burning velocity measurements using the Heat Flux method and numerical predictions of iso-octane/ethanol blends for different preheat temperatures. *Fuel* **2015**, *140*, 10–16. [CrossRef]
34. Chong, C.T.; Hochgreb, S. Measurements of laminar flame speeds of acetone/methane/air mixtures. *Combust. Flame* **2011**, *158*, 490–500. [CrossRef]
35. Gong, C.; Li, Z.; Li, D.; Liu, J.; Si, X.; Yu, J.; Huang, W.; Liu, F.; Han, Y. Numerical investigation of hydrogen addition effects on methanol-air mixtures combustion in premixed laminar flames under lean burn conditions. *Renew. Energy* **2018**, *127*, 56–63. [CrossRef]
36. Wu, Y.; Modica, V.; Rossow, B.; Grisch, F. Effects of pressure and preheating temperature on the laminar flame speed of me-thane/air and acetone/air mixtures. *Fuel* **2016**, *185*, 577–588. [CrossRef]
37. Zhang, Z.; Zhu, S.; Liang, J.; Tian, L.; Li, G. Experimental and kinetic studies of premixed laminar flame of ace-tone-butanol-ethanol (ABE)/air. *Fuel* **2018**, *211*, 95–101. [CrossRef]
38. Zhang, S.; Lee, T.H.; Wu, H.; Pei, J.; Wu, W.; Liu, F.; Zhang, C. Experimental and kinetic studies on laminar flame characteristics of ace-tone-butanol-ethanol (ABE) and toluene reference fuel (TRF) blends at atmospheric pressure. *Fuel* **2018**, *232*, 755–768. [CrossRef]
39. Xu, C.; Wang, H.; Zhou, K.; Li, X.; Zhou, W.; Liu, W.; Wang, C. Laminar Burning Velocity of Premixed Ethanol–Air Mixtures with La-ser-Induced Spark Ignition Using the Constant-Volume Method. *Energy Fuels* **2019**, *33*, 7749–7758. [CrossRef]
40. Xu, C.; Wu, S.; Oppong, F.; Xie, C.; Wei, L.; Zhou, J. Experimental and numerical studies of laminar flame characteristics of ethyl acetate with or without hydrogen addition. *Int. J. Hydrog. Energy* **2020**, *45*, 20391–20399. [CrossRef]
41. Xu, C.; Zhong, A.; Li, X.; Wang, C.; Sahu, A.; Xu, H.; Lattimore, T.; Zhou, K.; Huang, Y. Laminar burning characteristics of upgraded biomass pyrolysis fuel de-rived from rice husk at elevated pressures and temperatures. *Fuel* **2017**, *210*, 249–261. [CrossRef]
42. Xu, C.; Zhong, A.; Wang, H.; Jiang, C.; Sahu, A.; Zhou, W.; Wang, C. Laminar burning velocity of 2-methylfuran-air mixtures at ele-vated pressures and temperatures: Experimental and modeling studies. *Fuel* **2018**, *231*, 215–223. [CrossRef]
43. Xu, C.; Wang, H.; Li, X.; Zhou, W.; Wang, C.; Wang, S. Explosion characteristics of a pyrolysis biofuel derived from rice husk. *J. Hazard. Mater.* **2019**, *369*, 324–333. [CrossRef] [PubMed]
44. Yu, H.; Han, W.; Santner, J.; Gou, X.; Sohn, C.H.; Ju, Y.; Chen, Z. Radiation-induced uncertainty in laminar flame speed measured from propagating spherical flames. *Combust. Flame* **2014**, *161*, 2815–2824. [CrossRef]
45. Liao, S.; Jiang, D.; Huang, Z.; Zeng, K.; Cheng, Q. Determination of the laminar burning velocities for mixtures of ethanol and air at elevated temperatures. *Appl. Therm. Eng.* **2007**, *27*, 374–380. [CrossRef]
46. Law, C.K. *Combustion Physics*; Cambridge University Press (CUP): Cambridge, UK, 2006.
47. Van Geem, K.M.; Cuoci, A.; Frassoldati, A.; Pyl, S.P.; Marin, G.B.; Ranzi, E. An Experimental and Kinetic Modeling Study of Pyrolysis and Combustion of Acetone-Butanol-Ethanol (Abe) Mixtures. *Combust. Sci. Technol.* **2012**, *184*, 942–955. [CrossRef]
48. Yan, B.; Cheng, Y.; Li, T.; Cheng, Y. Detailed kinetic modeling of acetylene decomposition/soot formation during quenching of coal pyrolysis in thermal plasma. *Energy* **2017**, *121*, 10–20. [CrossRef]

49. Jiang, Y.; del Alamo, G.; Gruber, A.; Bothien, M.R.; Seshadri, K.; Williams, F.A. A skeletal mechanism for prediction of ignition delay times and laminar premixed flame velocities of hydrogen-methane mixtures under gas turbine conditions. *Int. J. Hydrog. Energy* **2019**, *44*, 18573–18585. [CrossRef]
50. Di Sarli, V.; Di Benedetto, A. Laminar burning velocity of hydrogen-methane/air premixed flames. *Int. J. Hydrog. Energy* **2007**, *32*, 637–646. [CrossRef]
51. Tsang, W. Energy transfer effects during the multichannel decomposition of ethanol. *Int. J. Chem. Kinet.* **2004**, *36*, 456–465. [CrossRef]
52. Tran, L.-S.; Glaude, P.-A.; Fournet, R.; Battin-Leclerc, F. Experimental and Modeling Study of Premixed Laminar Flames of Ethanol and Methane. *Energy Fuels* **2013**, *27*, 2226–2245. [CrossRef] [PubMed]
53. Li, Y.; Chen, Y.; Wu, G. Skeletal Mechanism Generation and Validation for Acetone–n-butanol–ethanol (ABE) Combustion in Diesel Engine. *Energy Fuels* **2020**, *34*, 965–980. [CrossRef]